Available online at www.sciencedirect.com
ScienceDirect
Trans. Nonferrous Met. Soc. China 32(2022) 424−435
Transactions of Nonferrous Metals Society of China
www.tnmsc.cn

Microstructures and corrosion behaviors of Al−6.5Si−0.45Mg−*x*Sc casting alloy

Yu-kun MA, Ming-xing WANG, Ya-nan LIU, Bin CAI

School of Physics and Microelectronics, Key Laboratory of Materials Physics of Ministry of Education, Zhengzhou University, Zhengzhou 450001, China

Received 30 January 2021; accepted 15 August 2021

Abstract: The microstructures and corrosion behaviors of the Al−6.5Si−0.45Mg casting alloys with the addition of Sc were investigated by using scanning electron microscopy, X-ray diffraction, electrochemical measurement techniques and immersion corrosion tests and compared with those of Sr-modified alloy. The results show that Sc has evident refining and modifying effects on the primary α(Al) and the eutectic Si phase of the alloy, and the effects can be enhanced with the increase of Sc content. When the Sc content is increased to 0.58 wt.%, its modifying effect on the eutectic Si is almost same as that of Sr. Sc can improve the corrosion resistance of the test alloy in NaCl solution when compared with Sr, but the excessively high Sc content cannot further increase the corrosion resistance of the alloy. The corrosion of the alloys mainly occurs in the eutectic region of the alloy, and mostly the eutectic α(Al) is dissolved. This confirms that Si phase is more noble than α(Al) phase, and the galvanic couplings can be formed between the eutectic Si and α(Al) phases.

Key words: Al−Si−Mg casting alloy; scandium (Sc); α(Al) phase; eutectic Si phase; corrosion resistance

1 Introduction

Al−Si−Mg casting alloy has many advantages, such as good mechanical properties and specific strength, excellent fluidity and castability, and good corrosion resistance. So, it has widely been used in the automotive and aerospace industries [1,2]. The mechanical properties of Al−Si−Mg casting alloys mainly depend on the morphology and distribution of the primary α(Al) phase and eutectic Si phase in the microstructure of the alloys. The primary α(Al) phase usually presents big dendritic structure, and the eutectic Si phase exhibits a very coarse plate-like morphology in the microstructures of untreated Al−Si casting alloys [3]. These microstructural characteristics greatly deteriorate the mechanical properties of the alloys, especially ductility [4]. The morphologies of the primary α(Al) phase and the eutectic Si phase can significantly be changed by adding grain-refining agent, such as Al−Ti, Al−Ti−B or Al−Ti−C master alloys, and eutectic Si modifying agents, such as sodium and strontium, to the alloy melts before casting, leading to significant improvement in the mechanical properties of Al−Si−Mg casting alloys [5,6]. However, good grain-refining and modifying effects can be achieved only when the grain-refining agents and modifying agents are simultaneously added to the alloy, and the effects degenerate after a prolonged holding time of the alloy melt [7,8]. Besides, the joint addition of the grain-refining agent containing boron together with the Sr-modifier may result in the formation and settling of SrB_6 particles [9,10], as a result, reducing the available amount of Sr for modifying the eutectic Si in the alloy melts.

In recent years, the roles of Sc in Al−Si−Mg

Corresponding author: Ming-xing WANG, Tel: +86-13525568755, E-mail: wangmx@zzu.edu.cn
DOI: 10.1016/S1003-6326(22)65804-7

casting alloys have been studied [11−19], and the existing studying results suggest that Sc has both refining and modifying effects on the primary α(Al) phase and eutectic Si phase of Al−Si−Mg casting alloys. PRAMOD et al [11] found that the addition of 0.4 wt.% Sc to the A356 casting alloy resulted in a 50% reduction in the secondary dendritic arm spacing and changed the morphology of eutectic Si from plate-like to fibrous and globular. PANDEE et al [18] and XU et al [19] claimed that the addition of Sc significantly refined both the primary α(Al) grain size and the eutectic silicon particle size of the Al−Si−Mg casting alloys.

The addition of the grain-refining and the modifying agents to Al−Si−Mg casting alloys changes the microstructures of the alloys [20], while it can also significantly affect the corrosion resistance of the alloys. LEE et al [21] found that the addition of 200×10^{-6} Sr to the A356 alloy could increase the galvanic couplings, resulting in high corrosion current density of the pitting corrosion at eutectic α(Al) of the inter-dendritic region in 3.5 wt.% NaCl solution. FARAHANY et al [22] pointed out that Bi, Sb and Sr elements could refine the eutectic Si of the Al−11Si−2Cu−0.8Zr die cast alloy, but also have a detrimental effect on the corrosion rate of the alloy. ÖZTURK et al [23] suggested that the corrosion resistance of the A356 alloy was improved through Sr addition. DUYGUN et al [24] found that the corrosion current density and corrosion resistance values of the Al−9wt.%Si alloy with addition of Sr in NaCl solution were more stable than those of the unmodified alloy. OSÓRIO et al [25] pointed out that the corrosion resistance of Na-modified Al−9wt.%Si alloy in NaCl solution tended to decrease when compared with the unmodified alloy. CARDINALE et al [2] suggested that the addition of different rare-earth elements to Al−Si casting alloy caused the formation of a protective rare-earth oxide-hydroxide film on alloy surface with the increase of exposure time in the NaCl solution. ZOU et al [26] found that the corrosion resistance of the hypoeutectic Al−Si alloy with addition of Yb in NaCl solution was very good. As for the effect of Sc on the corrosion resistance of Al−Si−Mg casting alloy, there have yet been few studies so far.

Therefore, in this study, the microstructural characteristics and corrosion behaviors of the Al−6.5Si−0.45Mg casting alloys with the different contents of Sc were investigated by using scanning electron microscope (SEM), X-ray diffraction (XRD), electrochemical impedance spectroscopy (EIS), potentiodynamic polarization techniques and immersion corrosion tests in 3.5 wt.% NaCl solution at room temperature and compared with those of Sr-modified alloy.

2 Experimental

All the test alloys were prepared in a pit-type resistance furnace. The starting materials include 99.9 wt.% high purity Al, pure Si and Al−50wt.%Mg, Al−2wt.%Sc and Al−10wt.%Sr master alloys. The pure Al ingots were firstly placed to a graphite crucible in the furnace and melted. The proper amount of pure Si and the master alloys were then added to the Al melt according to the desired composition of the test alloys when the Al melt was heated up to (740±5) °C. The alloy melts were fully stirred after the pure Si and master alloys were completely melted, and degased for 5 min using argon gas at (730±5) °C. The alloy melts were finally poured into a preheated ((200±5) °C) steel mold with dimensions of 80 mm in depth and 30 mm in internal diameter at (720±5) °C. For comparing, Sr-modified Al−Si−Mg alloy was also prepared in the same procedure. The alloy samples for microstructure analyses and corrosion test studies were cut off at (30±2) mm from the bottom of the alloy castings. The chemical compositions of all the alloy samples were analyzed by using Metalscan 2500 metals analyzer, and the results are listed in Table 1. The alloy samples were successively abraded with silicon carbide (SiC) emery papers up to 3000# followed by ultrasonic treatment, anhydrous ethanol cleaning and air drying for examining the microstructure as well as for the XRD studies. Cold field emission SEM attached with EDAX (JSM−6700F) was employed

Table 1 Chemical compositions of test alloys (wt.%)

Alloy	Si	Mg	Sc	Sr	Al
AS0	6.56	0.43	0	0.04	Bal.
AS1	6.67	0.45	0.13	0	Bal.
AS2	6.76	0.45	0.28	0	Bal.
AS3	6.50	0.41	0.45	0	Bal.
AS4	6.60	0.43	0.58	0	Bal.

to observe the microstructures and to examine the chemical elemental distribution of the alloy samples. Bruker-D8 Advance instrument with Cu K_α radiation was used to scan the alloy samples. The scanning speed was 5 (°)/min and the scanning range was of 20°−80°.

Electrochemical studies included EIS measurement and potentiodynamic polarization curve measurement. Electrochemical measurements were carried out by using CHI660E electrochemical workstation and a conventional three-electrode cell in 3.5 wt.% NaCl solution at room temperature. The alloy samples with a surface area of 1 cm^2 were used as working electrodes. A platinum electrode with the dimensions of 10 mm × 10 mm × 0.2 mm and a saturated calomel electrode (SCE) were used as counter electrode and reference electrode, respectively. The ratio of liquid volume to sample surface area was more than 100 mL/cm^2 in the cell. The alloy samples were firstly immersed in the solution for 1 h to establish the stable open-circuit potential (φ_{ocp}). When the alloy samples reached the stable φ_{ocp}, potentiodynamic polarization curves were recorded by sweeping the electrode potential from φ_{OCP} to −250 mV and to 250 mV at a scanning rate of 1.0 mV/s. Corrosion potential (φ_{corr}) and corrosion current density (J_{corr}) were calculated by the Tafel extrapolation method. EIS measurements were conducted at the φ_{ocp} by using a sinusoidal potential signal with a frequency range of 100 kHz to 0.05 Hz and voltage RMS of 5 mV, and 12 points per decade were taken during EIS measurements. In order to ensure the reliability of the electrochemical measurement results, at least two samples were tested for each alloy, and the measurement results of the two samples should basically be the same, otherwise another sample was tested. The impedance spectra were fitted using the ZView electrochemical analysis software by selecting appropriate circuits.

Immersion corrosion tests were also performed in 3.5 wt.% NaCl solution at room temperature. The alloy samples with the dimensions of 10 mm × 10 mm × 3 mm for immersion corrosion tests were prepared using the same procedure mentioned above, and immersed for 5, 10, 15 and 20 d in 3.5 wt.% NaCl solution, respectively. When an assigned immersion corrosion duration was reached, the alloy samples were taken out from the NaCl solution and treated in a solution of 20 g/L chromic oxide + 50 mL/L phosphoric acid at (80±2) °C for 3 min to remove the corrosion products. The mass losses of the alloy samples before and after immersion corrosion test were measured using a high precision scale with an accuracy of 0.01 mg, and the corrosion rate was calculated by Eq. (1) according to the ASTM G1-03 standard [27]:

$$C_r = K\frac{m}{ATD} \tag{1}$$

where C_r represents the corrosion rate (mm/a), K is a constant (6.78×10^4), m is the mass loss (g), A is the area of exposure in the NaCl solution (cm^2), T is the time of immersion (h), and D is the density of the alloy (g/cm^3). Three sets of samples were performed for immersion corrosion tests of each alloy. The corrosion rate value of each alloy was the average of the corrosion rates of the three samples, and the error ranges were also calculated based on the test results of the three samples. The surface morphologies of the alloy samples after 20 d of immersion in 3.5wt.% NaCl solution were observed using the SEM.

3 Results and discussion

3.1 Microstructure

To understand the effect of Sc on the microstructural characteristics and the distribution of the alloy elements in the Al−6.5Si−0.45Mg casting alloy, the microstructures and elemental distribution of the alloy samples with the addition of Sc or Sr were observed by the SEM attached EDAX, and the results are shown in Figs. 1 and 2, respectively. As can be seen from Fig. 1 that the microstructures of all the alloy samples consist of the primary α(Al) phases and the eutectic regions. The primary α(Al) phases of the Sr-modified alloy (AS0) present big dendrite morphology and the eutectic Si phases exhibit the fine fibrous structure (see Fig. 1(a)), which is quite different from the morphology of the coarse plate-shaped eutectic Si phase in the Al−Si casting alloy without modification treatment [15]. This indicates that Sr element has a good modifying effect on the eutectic Si, but does not have refinement effect on the primary α(Al) phases of the Al−6.5Si−0.45Mg casting alloy. For the alloy samples with the addition of Sc, the morphologies of the primary

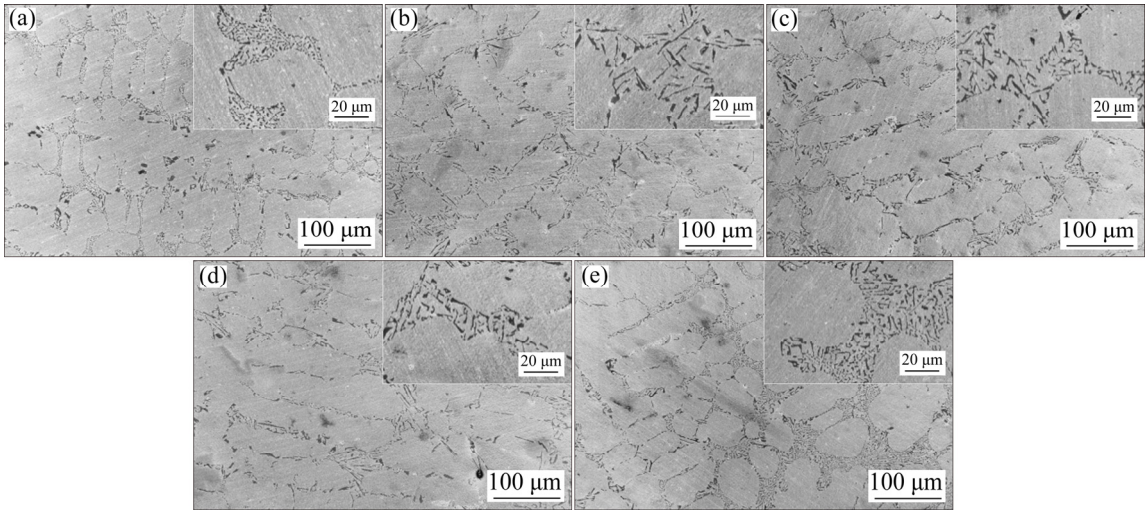

Fig. 1 SEM images of of Al−6.5Si−0.45Mg casting alloys with addition of Sc or Sr: (a) AS0; (b) AS1; (c) AS2; (d) AS3; (e) AS4

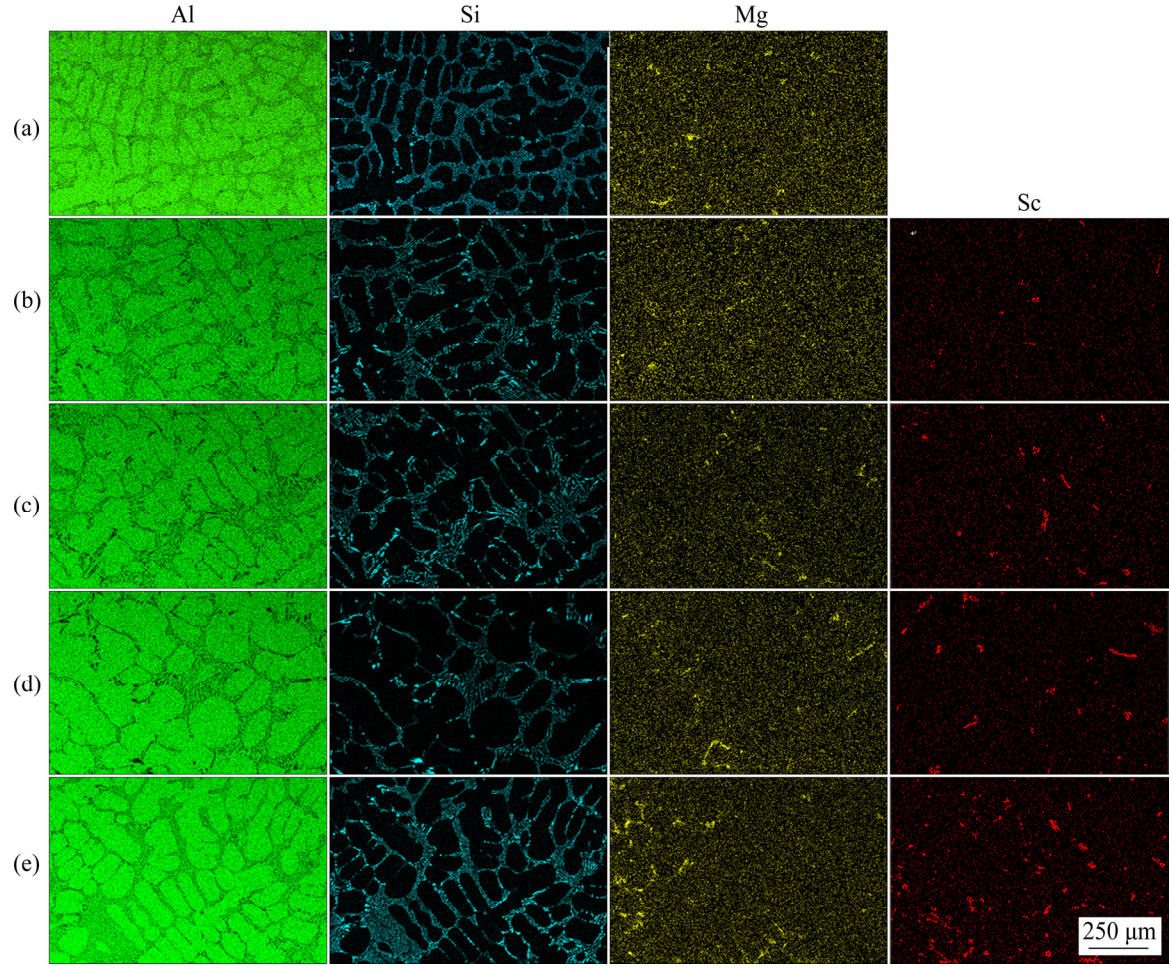

Fig. 2 EDAX elemental distribution mappings of alloy samples: (a) AS0; (b) AS1; (c) AS2; (d) AS3; (e) AS4

α(Al) phases have no obvious change and still present dendritic structures, but the morphologies of the eutectic Si phases are gradually transformed from coarse acicular to little rod- or worm-like shape when the addition content of Sc is increased from 0.13 to 0.45 wt.% (AS1, AS2, AS3) (see

Figs. 1(b, c, d)). When the addition content of Sc is further increased to 0.58 wt.% (AS4), the α(Al) phases are significantly refined, and the morphologies of the eutectic Si are also modified to fine fibrous or granular shapes (see Fig. 1(e)), which are very similar to that of the eutectic Si phases in the sample AS0. Sc can refine the α(Al) phase of Al−Si−Mg casting alloy mainly because Al_3Sc phase particles precipitate in advance during solidification of the alloy melts [13,17,19]. The crystal structure of Al_3Sc is very similar to that of Al, so it can act as the heterogeneous nucleation sites of Al, refining the α(Al) phase of the alloy [17]. There are no sufficient Al_3Sc phase particles formed in the alloy melts when the Sc content is relatively low, thus the refining effect is not very obvious. Good refining effect needs relatively high Sc content [13]. Therefore, the morphologies of the primary α(Al) phases of AS1, AS2 and AS3 are similar and present dendritic structures because of their relatively low Sc content. But the refinement of the α(Al) phase of the alloy with the addition of 0.58 wt.% Sc is very obvious because it has the highest Sc content among all the test alloy (see Fig. 1(e)). Modification of the eutectic Si with Sc is consistent with the impurity-induced twinning (IIT) modification mechanism, it is also related to the Sc content of the alloy [19].

The dendritic structure characteristics of the primary α(Al) phases of the alloy sample AS0, AS1, AS2 and AS3 can also be identified from the EDAX elemental distribution mapping shown in Figs. 2(a−d), and the equiaxed characteristics of the primary α(Al) phases of the alloy sample AS4 is also obvious (see Fig. 2(e)). These results indicate that the addition of little amount of Sc cannot evidently refine the primary α(Al) phases of the Al−6.5Si−0.45Mg casting alloy, but has a certain modifying effect on the eutectic Si phases of the alloy. The addition of a relatively high content of Sc can not only have evident refinement action on the primary α(Al) phases of the Al−6.5Si−0.45Mg casting alloy, but also have a good modifying effect on the eutectic Si phase. As for Si element, it is known from Al−Si phase diagram [28] that the solubility of Si in Al is of 1.65 wt.% at eutectic temperature of 577 °C, but only 0.05 wt.% at room temperature. Just because of the very low solubility of Si in Al, the Si mainly presents as pure Si phase in the eutectic regions of the alloys (see Fig. 2). In addition to the Si, the elemental distribution results indicate that the distribution of Mg is relatively homogeneous, but there are some distributions at the α(Al) grain boundaries of the alloys. The Sc element is also mostly presented at the primary α(Al) grain boundaries of the alloys, and there is a relative concentration of the Sc element with the increase of Sc content. EDAX analyses were performed at the locations of the Mg and Sc concentration in the samples AS3 and AS4, and the EDAX patterns are shown in Fig. 3. It is seen that the location of the Mg concentration should be the presence of Mg_2Si phase (see Fig. 3(a)), whilst the location of the Sc concentration is reasonably speculated as Al_3Sc phase based on the mass ratio of the examined Al to Sc content (see Fig. 3(b)).

In order to identify the phases, XRD analyses were carried out for the test alloys, and the XRD patterns are shown in Fig. 4. As can be seen from Fig. 4 that there are α(Al), Si and Mg_2Si phases for all the test alloys, the α(Al) peaks appear at 38.60°, 44.83°, 65.18° and 78.30° (ICDD-01-089-2837), the Si phases at 28.49°, 56.02°, 68.99° and 76.08° (ICDD-01-089-5012) and the Mg_2Si phases at 40.12°, 47.43° (ICDD-00-001-1192). At 58.15° (ICDD-01-073-1148), there is a weak peak of $Al_{12}Mg_{17}$ phase for the samples AS3 and AS4. A weak Al_3Sc peak appears at 33.49° (ICDD-00-017-0412) only for the sample AS4, but there is not any Al_3Sc peak presenting in the XRD pattern of the other alloy samples. It should be attributed to their very low concentration level in the alloys.

3.2 Corrosion behavior

3.2.1 Electrochemical corrosion behavior

To study the electrochemical corrosion behaviors of the test alloys, the EIS measurements were performed for the alloy samples after 1 h of immersion in 3.5 wt.% NaCl solution at room temperature, and the results are represented as Nyquist, Bode impedance and Bode phase angle plots in Fig. 5. It can be seen from Fig. 5(a) that the Nyquist plots exhibit a semi-circle capacitive arc for the samples AS1, AS2 and AS4, and a capacitive arc and an inductive arc for the samples AS0 and AS3. It is well known that the diameter of the capacitive arc indicates the corrosion resistance of the alloys, and the big diameter represents a good corrosion resistance [23,29]. The diameters of the

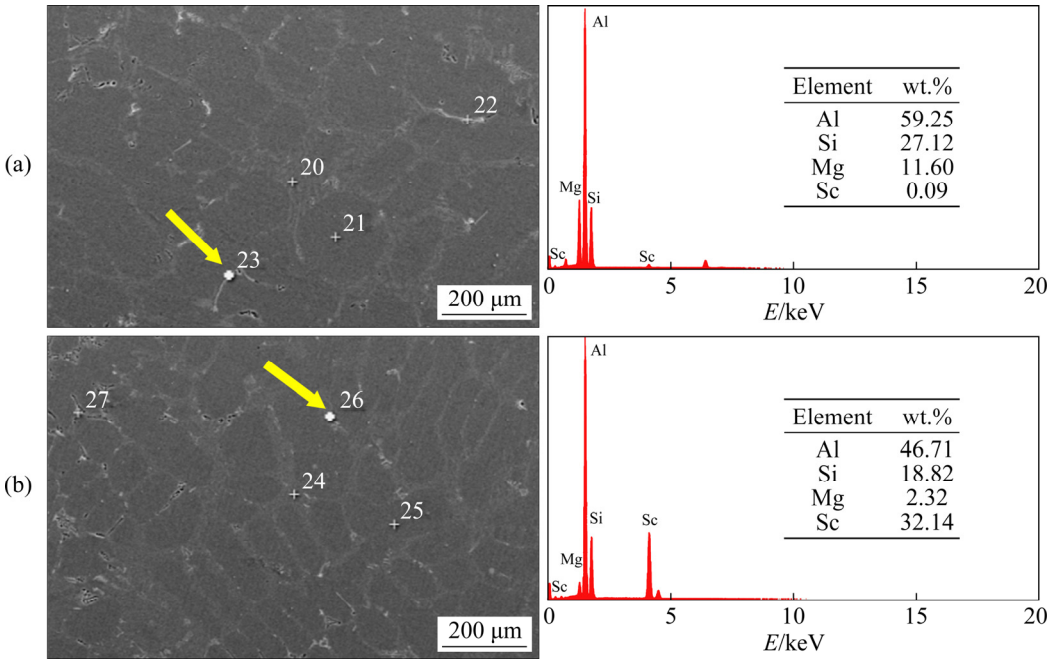

Fig. 3 EDAX patterns at locations of Mg and Sc concentration: (a) Mg concentration in AS3; (b) Sc concentration in AS4

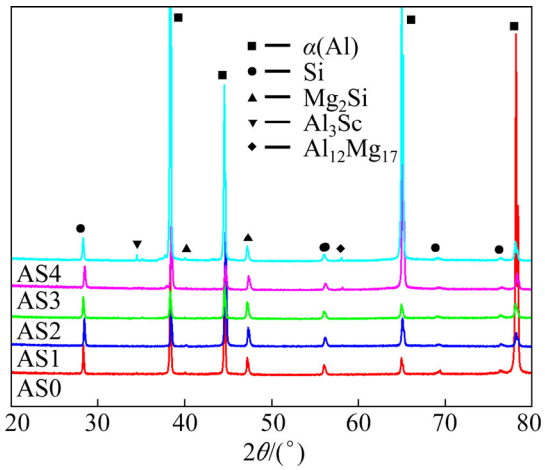

Fig. 4 XRD patterns of test alloy samples

capacitive arc of the samples AS2, AS1, AS3, AS0 and AS4 decrease successively, indicating that their corrosion resistances are successively weakened. High impedance value (|*Z*|) in Bode impedance plot at low frequency region is an indication of good corrosion resistance of the alloys [30]. It is seen from Bode impedance plots (see Fig. 5(b)) that the slope of the plots at the middle frequency region successively decreases for the samples AS2, AS1, AS3, AS0 and AS4. The impedance value (|*Z*|) at low frequency range also successively decreases, the change law of which is consistent with that of the diameter of the capacitive arc. Therefore, it can be concluded that the corrosion resistance of the samples AS2, AS1, AS3 is better than that of the samples AS0 and AS4, and the sample AS2 has the best corrosion resistance. The Nyquist plots of the samples AS0 and AS3 have an inductive arc. The appearance of inductive arc generally indicates the existence of unstable conditions in the corroding substrate and the relaxation process of adsorbed corrosion intermediates, and can accelerate the α(Al) dissolution [31]. Bode phase angle plots (see Fig. 5(c)) basically represents the change in the capacitive behavior. The peak value and area in the frequency range of 10^3 to 1 Hz for the samples AS2, AS1, AS3, AS0 and AS4 are successively decreased. It confirms the decrease of capacitive behavior and breakdown of the surface layer. The phase angle values of the samples AS0 and AS3 decreasing to below 0° at 0.05 Hz indicates the ingress of aggressive ions through the surface layer and accelerates the α(Al) dissolution with multiple reaction kinetics. The phase angle maxima and peak area of the alloy sample AS2 are the highest, whilst the samples AS0 and AS3 exhibit inductive behavior due to their higher reactivity in the low frequency region.

More information about the corrosion mechanism of the test alloys can be obtained through fitting the EIS data with proper equivalent

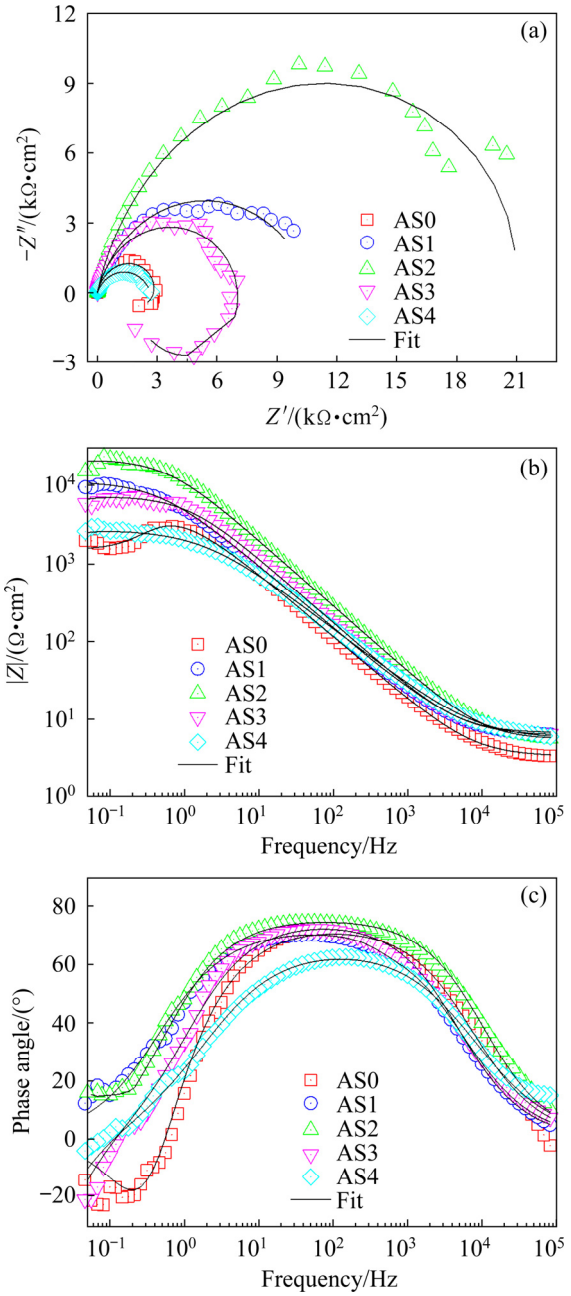

Fig. 5 EIS results of test alloy samples: (a) Nyquist plots; (b) Bode impedance plots; (c) Bode phase angle plots

circuit (EC) models. In order to obtain a high precision fitting results, two types of EC models, as shown in Fig. 6, were used for fitting the EIS data [31], the EC model shown in Fig. 6(a) for AS1, AS2 and AS4, and the EC model in Fig. 6(b) for AS0 and AS3. The circuit parameters of the EC models include solution resistance (R_s), surface layer resistance (R_1), charge transfer resistance (R_2), constant phase elements (CPE) of surface layer (Q_1) and double layer (Q_2), inductance (L) and inductance resistance (R_L). CPEs with coefficients n_1 and n_2 are used instead of capacitance to show the deviation from the ideal capacitive behavior [32]. The circuit parameters obtained from curve fitting for the EIS data are listed in Table 2. As can be seen from Table 2 that, the R_1 value of the sample AS2 is 29.68 kΩ·cm^2 and successively decreases to 11.41 and 2.58 kΩ·cm^2 for the samples AS1 and AS4, respectively. There is not R_1 value for

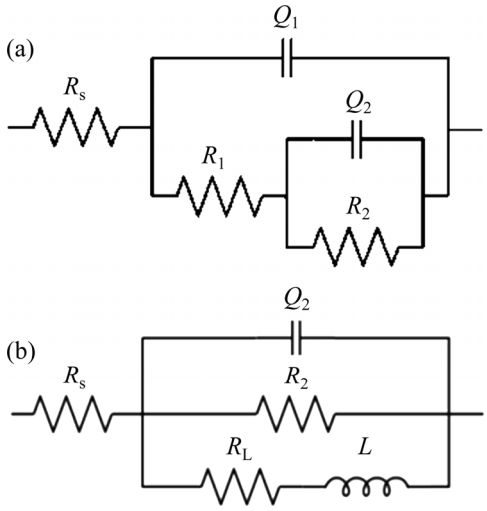

Fig. 6 Equivalent circuit models used for curve fitting of EIS results for AS1, AS2 and AS4 (a), and for AS0 and AS3 (b)

Table 2 Circuit parameters obtained from fitting for EIS data of test alloys

Alloy	R_s/ (Ω·cm^2)	Q_1/ (μSs^n·cm^{-2})	n_1	R_1/ (kΩ·cm^2)	Q_2/ (s^n·cm^{-2})	n_2	R_2/ (kΩ·cm^2)	L/ (H·cm^{-2})	R_L/ (kΩ·cm^2)	Chi-squared
AS0	5.29± 0.46	–	–	–	46.1± 1.5	0.82± 0.02	3.78± 0.39	1810± 127	2.13± 0.18	0.0011
AS1	6.15± 0.52	47.7± 2.8	0.73± 0.01	11.41± 1.01	37.3± 2.9	0.81± 0.01	10.75± 1.15	–	–	0.0015
AS2	5.36± 0.44	15.9± 1.6	0.83± 0.02	29.68± 1.45	15.3± 1.4	0.79± 0.01	26.87± 1.08	–	–	0.0024
AS3	6.48± 0.39	–	–	–	26.8± 1.8	0.84± 0.02	7.28± 0.66	67711± 952	2.28± 0.21	0.0013
AS4	5.53± 0.49	58.6± 3.3	0.74± 0.01	2.58± 0.19	63.8± 3.8	0.73± 0.01	2.59± 0.19	–	–	0.0028

the samples AS0 and AS3 because of their inductive behavior, but their R_L values are 2.13 and 2.28 kΩ·cm^2, respectively. The R_1 value is related to the compactness of the surface layer, and a higher R_1 value implies that the surface layer is more compact, and it is less likely destroyed in the corrosion environment [23]. A stable and compact surface layer can block the penetration of electrolyte and inhibit the further dissolution of the substrate [22]. The highest R_1 value and lowest Q_1 value of the sample AS2 imply that it has the best corrosion resistance. The charge transfer resistance (R_2) is a measure of electron transfer across the surface and inversely proportional to corrosion rate [23]. The high R_2 value and low Q_2 values indicate a better corrosion protective ability for the alloy samples. The R_1 value of the sample AS2 is the highest, and the R_2 values of the samples AS1 and AS3 are also higher than those of the samples AS0 and AS4. These further confirm that the corrosion resistances of the samples AS1, AS2 and AS3 are better than those of the samples AS0 and AS4, and AS2 has the best corrosion resistance among all the alloy samples.

It has been known from the microstructure analysis results mentioned above that the eutectic Si phases of the test alloys are gradually modified with the increase of the addition of Sc, and the addition of 0.58 wt.% Sc has a very good modifying effect, and is almost the same as that of the Sr element. The study of ÖZTÜRK et al [23] revealed that the formation of surface layer depended on the size and shape of eutectic Si phases, and the compact surface layer could be formed on the Al−Si alloy modified with Sr element, as a result, improving the corrosion resistance of the alloy compared with unmodified alloy. However, in this study, the EIS measurement results indicate that the R_1 value of the Sr-modified alloy (AS0), which reflects the property of the surface layer, is not noticed because of the inductive behavior. The morphology of the eutectic Si of the sample AS4 is similar to that of the sample AS0, whilst the R_1 value of it is also very low (see Table 3). This implies that a good surface layer cannot be formed on the Al−6.5Si−0.45Mg casting alloys with fine eutectic Si phase. The fine eutectic Si phases increase the interface between the eutectic Si and the eutectic α(Al) phases. It makes charge transfer easier, thus decreasing the charge transfer resistance R_2 value. Besides, the electrochemical activity of the alloy surfaces may also be increased due to the increase of the interface between the eutectic Si and the eutectic α(Al) phases. It may also increase the difficulty of the formation of surface layer. The coarse eutectic Si phase forms a heterogeneous surface structure, and it increases the difficulty of the formation of a stable surface layer on the alloys in aqueous solutions [33]. The eutectic Si phases of the sample AS1 are relatively coarse. It is responsible for the relative low R_1 value of the sample AS1. The microstructure of the sample AS2 is the most suitable for the formation of a stable surface layer, thus it has the best corrosion resistance.

Potentiodynamic polarization measurements were also carried out for the test alloys after 1 h of immersion in the 3.5 wt.% NaCl solution at room temperature, and the polarization curves are represented in Fig. 7. As can been seen from Fig. 7 that the polarization curves of the samples AS1, AS2 and AS3 are significantly shifted to the left compared with that of the alloy sample AS0, it implies that both the cathodic and anodic current densities of the samples AS1, AS2 and AS3 are all lower than those of the sample AS0, that is, they have lower cathodic and anodic reactions. Decrease of the reactions suggests the low dissolution rate of the alloys. Thus these alloy samples exhibit lower corrosion rate when compared with the sample AS0. The polarization curve of the sample AS4 is very similar to that of the sample AS0, indicating that

Table 3 Polarization parameters extracted from potentiodynamic polarization curves of test alloys

Alloy	φ_{corr}(vs SCE)/V	φ_b/V	J_{corr}/(μA·cm^2)	R_p/(kΩ·cm^2)
AS0	−0.686±0.004	−0.686±0.004	18.51±0.42	2.15±0.02
AS1	−0.813±0.007	−0.694±0.005	0.44±0.09	9.67±0.01
AS2	−0.73±0.01	−0.642±0.004	0.32±0.06	20.03±0.05
AS3	−0.769±0.008	−0.664±0.006	4.54±0.03	6.95±0.01
AS4	−0.688±0.004	−0.688±0.004	22.73±0.67	2.54±0.02

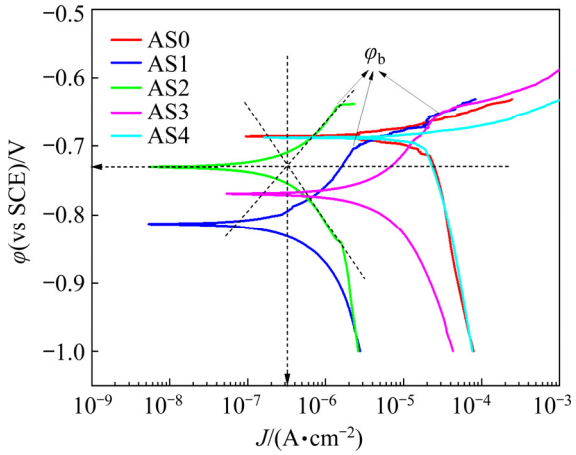

Fig. 7 Potentiodynamic polarization curves of test alloys after 1 h of immersion in 3.5 wt.% NaCl solution

they have similar corrosion rate. Besides, a rapid increase in the current density can be observed at the potentials of −0.694, −0.642 and −0.664 V in the anodic region of the polarization curves of the samples AS1, AS2 and AS3, respectively. This indicates the breakdown of the surface layer at the onset of the potential values, which is known as the breakdown potential φ_b (see Fig. 7). There are not evident breakdown onset in the anodic region of the polarization curves of the samples AS0 and AS4, indicating that the breakdown potential coincides with the corrosion potentials of the alloys. Therefore, although there are difference in the corrosion potential of the test alloy samples, the breakdown potential is relatively close to each other (see Fig. 7).

The corrosion potential and corrosion current density (J_{corr}) were extracted by the Tafel extrapolation method from the polarization curves shown in Fig.7, and the results are listed in Table 3. Additionally, the polarization resistance R_p was determined by using the Sterne−Geary equation, and also given in Table 3. It is seen from Table 3 that the J_{corr} values of the samples AS1, AS2 and AS3 are lower than those of the samples AS0 and AS4, and the J_{corr} value of the sample AS2 is the lowest among all the alloy samples. Therefore, the corrosion rates of the samples AS1, AS2 and AS3 are all lower than those of the samples AS0 and AS4, and the corrosion rate of the sample AS2 is the lowest among all the test alloys. A higher R_p value indicates the better corrosion resistance of the alloy [34]. The R_p values shown in Table 3 also reflect the change law in the corrosion resistance of the test alloys.

Due to the fine eutectic Si phases of the samples AS0 and AS4, more galvanic couplings can be formed in the alloys during immersing in the corrosion solution because the eutectic Si phase is more noble than the eutectic α(Al) phase around it, and can act as local cathodes with respect to the eutectic α(Al) phase compared with the samples AS1, AS2 and AS3 [33,35]. It is the reason that the samples AS0 and AS4 have high J_{corr} value. As for the Mg_2Si and Al_3Sc phases, the amount of the Mg_2Si phases precipitated at the α(Al) grain boundaries of all the test alloys is the same because of the nearly same content of Mg and Si in the alloys. Therefore, the Mg_2Si phases do not cause the difference in the corrosion resistance of the test alloys. The amount of the Al_3Sc phases increases with the increase of the Sc content. However, the study of CAVANATGH et al [36] revealed that Al_3Sc phase was slightly cathodic to the α-Al matrix of Al-alloys, and it displayed good electrochemical compatibility with Al-alloys. So Al_3Sc phase did not increase the susceptibility of corrosion of Al-alloys [36]. Therefore, the effect of the variation in the amount of Al_3Sc phases in the different test alloys on the corrosion rate should be very small. In this sense, the morphology and distribution of the eutectic Si phases should be a key factor affecting the corrosion resistance of the Al−6.5Si−0.45Mg casting alloy.

3.2.2 Immersion corrosion

In order to substantiate the results of the electrochemical corrosion behavior studies, the immersion corrosion tests of 5, 10, 15 and 20 d in 3.5 wt.% NaCl solution at room temperature, respectively, were performed for all the test alloys. The average corrosion rates of the alloy samples after immersion for different durations were calculated based on the mass loss before and after the immersion corrosion test, and the results are shown in Fig. 8. As can be seen from Fig. 8 that the corrosion rates of the samples AS1, AS2 and AS3 are all lower than those of the samples AS0 and AS4, and the sample AS2 has the lowest corrosion rate among all the alloy samples except for the immersion duration of 20 d. These results are basically in agreement with the electrochemical corrosion measurement results. The corrosion rate of the sample AS0 increases with the increase of the immersion duration from 5 to 10 d, but decreases

with further increase of the immersion duration. The increase of the immersion duration gradually destroys the natural oxide layer on the surface of the alloys, resulting in the increase in the corrosion rate of the alloy. As for the decrease of the corrosion rate of the alloy with further increase of the immersion duration, there may be two reasons: one is that with the fast dissolution of the eutectic α(Al) phase around the eutectic Si phases, the contacting area between the eutectic Si and α(Al) phases decreases, it surely decreases the rate of further dissolution of the eutectic α(Al) phases because of the reduction of the corrosion current density; the second is that the accumulation of the corrosion products on the alloy sample surface during immersion further inhibits dissolution of the alloy substrate. The corrosion rates of the samples AS1, AS2, AS3 and AS4 are all lower than that of the sample AS0. It indicates that the addition of Sc to the Al−6.5Si−0.45Mg casting alloy can improve the corrosion resistance of the alloys when compared with the addition of Sr element. Besides, the corrosion rates of the samples AS1, AS2, AS3 and AS4 basically increase with the increase of the immersion duration (see Fig. 8). It may be because the decrease in the contacting area between the eutectic Si and α(Al) phases and the accumulation of the corrosion products on the alloy surfaces have not reached the severity that can decrease the corrosion rate of the alloy samples for the immersion test duration of this study due to their relatively low corrosion rate.

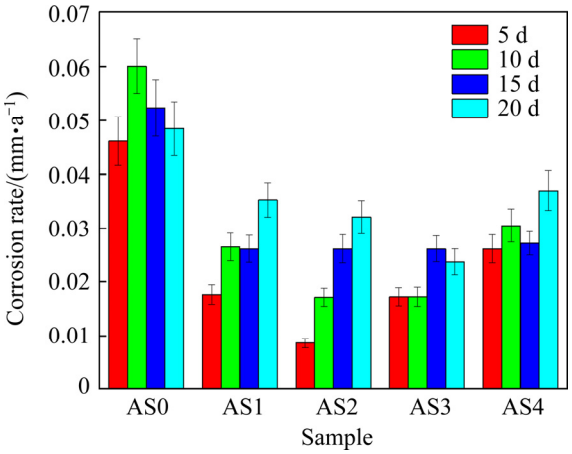

Fig. 8 Comparison of corrosion rates of alloys after 5, 10, 15 and 20 d of immersion in 3.5 wt.% NaCl solution

The surface morphologies of the samples after 20 d of immersion in the 3.5 wt.% NaCl solution were observed by the SEM and the results are shown in Fig. 9. As seen from Fig. 9 that the surface corrosion morphologies of all the alloy samples are similar, and no significant difference can be noticed. The dissolution of the α(Al) phases mainly occurs in the eutectic region between the primary α(Al) phases. The eutectic α(Al) phases around the eutectic Si phases are dissolved, but the eutectic Si phases are remained in the eutectic regions. It confirms that the Si phase is more noble than the α(Al) phase, and the galvanic couplings can be formed between the eutectic Si and α(Al) phases. Figure 9 also shows that the dissolution of the α(Al) phases in the eutectic region of the sample

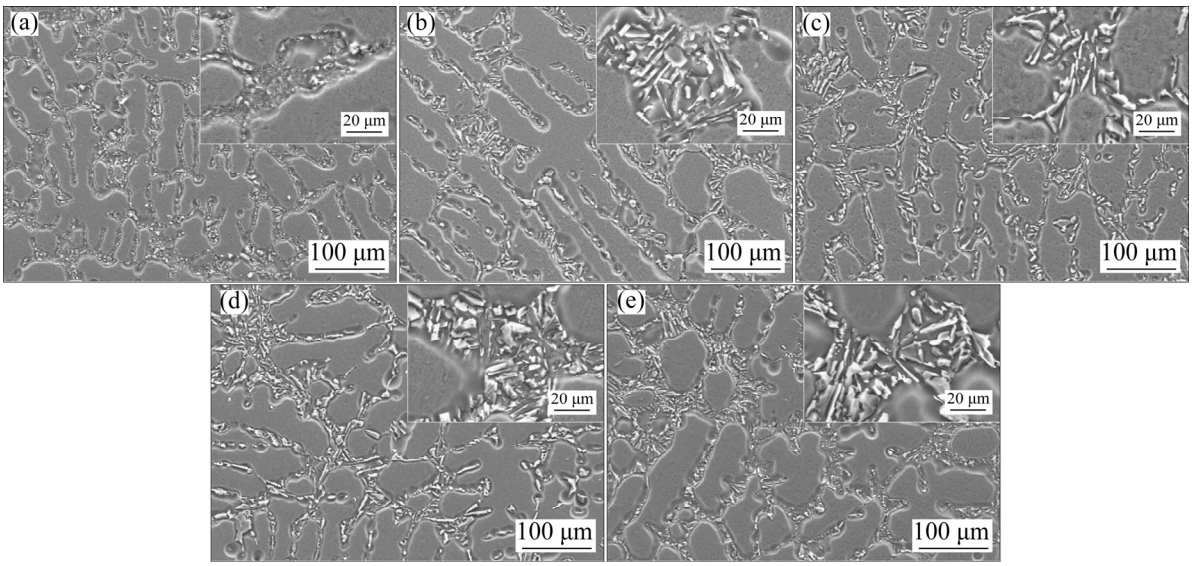

Fig. 9 SEM images of alloy surface after 20 d of immersion in 3.5 wt.% NaCl solution and after removing corrosion products: (a) AS0; (b) AS1; (c) AS2; (d) AS3; (e) AS4

AS0 seems to be more serious, indicating that it has the highest corrosion rate.

4 Conclusions

(1) Sc has an evident refining and modifying effects on the primary α(Al) and the eutectic Si phases of the Al−6.5Si−0.40Mg casting alloy, and the effects are enhanced with the increase of Sc content. When the Sc content is increased to 0.58 wt.%, its modifying effect on the eutectic Si phases is almost same as that of Sr element.

(2) The test alloys containing 0.13, 0.28 and 0.45 wt.% Sc (AS1, AS2 and AS3) exhibit higher surface layer resistance R_1 and/or charge transfer resistance R_2 compared with the Sr- and 0.58 wt.% Sc-modified alloys (AS0 and AS4) during the EIS measurements. Therefore, the corrosion resistances of AS1, AS2 and AS3 are all better than those of AS0 and AS4. The fine eutectic Si phases of AS0 and AS4 are responsible for the poor corrosion resistance.

(3) The potentiodynamic polarization measurement results reveal that AS1, AS2 and AS3 have lower corrosion current density and higher polarization resistance than AS0 and AS4. This indicates that Sc can decrease the corrosion rate of the Al−6.5Si−0.45Mg casting alloy compared with Sr. But the excessively high Sc content cannot further decrease the corrosion rate of the samples although it can exhibit better refining and modifying effects on the primary α(Al) and eutectic Si phases of the alloy.

(4) The immersion corrosion tests substantiate that the corrosion rates of AS1, AS2 and AS3 are lower than those of AS0 and AS4. The corrosion mainly occurs in the eutectic region of the alloys during the immersion, and mostly the eutectic α(Al) phases are dissolved, but the eutectic Si phases are remained in the eutectic region. It confirms that the Si phase is more noble than the α(Al) phase, and the galvanic couplings can be formed between the eutectic Si and α(Al) phases.

References

[1] MILLER W S, ZHUANG L, BOTTEMA J, WITTEBROOD A J, de SMET P D, HASZLER A, VIEREGGE A. Recent development in aluminium alloys for the automotive industry [J]. Materials Science and Engineering A, 2000, 280(1): 37−49.

[2] CARDINALEA M, MACCIÒ D, LUCIANO G, CANEPA E, TRAVERSO P. Thermal and corrosion behavior of as cast AlSi alloys with rare earth elements [J]. Journal of Alloys and Compounds, 2017, 695: 2180−2189.

[3] OSÓRIO W R, GARCIA R L, GOULART P R, GARCIA A. Effects of eutectic modification and T4 heat treatment on mechanical properties and corrosion resistance of an Al−9wt.%Si casting alloy [J]. Materials Chemistry and Physics, 2007, 106(2/3): 343−349.

[4] HEUSLER L, SCHNEIDER W. Influence of alloying elements on the thermal analysis results of Al−Si cast alloys [J]. Journal of Light Metals, 2002, 2(1): 17−26.

[5] ASENSIO-LOZANO J, SUAREZ-PEÑA B. Effect of the addition of refiners and/or modifiers on the microstructure of die cast Al−12Si alloys [J]. Scripta Materialia, 2006, 54(5): 943−947.

[6] LU L, NOGITA K, DAHLE A K. Combining Sr and Na additions in hypoeutectic Al−Si foundry alloys [J]. Materials Science and Engineering A, 2005, 399(1/2): 244−253.

[7] LIMMANEEVICHITR C, EIDHED W. Fading mechanism of grain refinement of aluminum-silicon alloy with Al−Ti−B grain refiners [J]. Materials Science and Engineering A, 2003, 349(1/2): 197−206.

[8] SCHAFFER P L, DAHLE A K. Settling behavior of different grain refiners in aluminium [J]. Materials Science and Engineering A, 2005, 413/414: 373−378.

[9] BIROL Y. Interaction of grain refinement with B and modification with Sr in aluminium foundry alloys [J]. Materials Science and Technology, 2012, 28(1): 70−76.

[10] LU L, DAHLE A K. Effects of combined additions of Sr and AlTiB grain refiners in hypoeutectic Al-Si foundry alloys [J]. Materials Science and Engineering A, 2006, 435/436: 288−296.

[11] PRAMOD S L, PRASADA RAO A K, MURTY B S, BAKSHI S R. Effect of Sc addition on the microstructure and wear properties of A356 alloy and A356−TiB_2 in situ composite [J]. Materials and Design, 2015, 78: 85−94.

[12] ZHANG W D, LIU Y, YANG J, DANG J Z, XU H, DU Z M. Effects of Sc content on the microstructure of as-cast Al−7wt.%Si alloys [J]. Materials Characterization, 2012, 66: 104−110.

[13] KAISER M S, BASHER M R, KURNY A S W. Effect of scandium on microstructure and mechanical properties of cast Al−Si−Mg alloy [J]. Journal of Materials Engineering and Performance, 2012, 21(7): 1504−1508.

[14] TZENG Y C, WU C T, BOR H Y, HORNG J L, TSAI M L, LEE S L. Effects of scandium addition on iron-bearing phases and tensile properties of Al–7Si–0.6Mg alloys [J]. Materials Science and Engineering A, 2014, 593: 103−110.

[15] PRAMOD S L, RAVIKIRANA, PRASADA RAO A K, MURTY B S, BAKSHI S R. Effect of Sc addition and T6 aging treatment on the microstructure modification and mechanical properties of A356 alloy [J]. Materials Science and Engineering A, 2016, 674: 438−450.

[16] LU Z, ZHANG L J. Thermodynamic description of the quaternary Al−Si−Mg−Sc system and its application to the design of novel Sc-additional A356 alloys [J]. Materials and Design, 2017, 116: 427−437.

[17] PATAKHAM U, KAJORNCHAIYAKUL J, LIMMANEEVICHITR C. Grain refinement mechanism in an Al−Si−Mg alloy with scandium [J]. Journal of Alloys and Compounds, 2012, 542: 177−186.
[18] PANDEE P, GOURLAY C M, BELYAKOV S A, PATAKHAM U, ZENG G, LIMMANEEVICHITR C. $AlSi_2Sc_2$ intermetallic formation in Al−7Si−0.3Mg−*x*Sc alloys and their effects on as-cast properties [J]. Journal of Alloys and Compounds, 2018, 731: 1159−1170.
[19] XU C, XIAO W L, HANADA S, YAMAGATA H, MA C L. The effect of scandium addition on microstructure and mechanical properties of Al−Si−Mg alloy: A multi-refinement modifier [J]. Materials Characterization, 2015, 110: 160−169.
[20] HAQUE M M, ISMAIL A F. Effect of superheating temperatures on microstructure and properties of strontium modified aluminium–silicon eutectic alloy [J]. Journal of Materials Processing Technology, 2005, 162/163: 312−316.
[21] LEE S L, CHENG Y C, CHEN W C, LEE C K, TAN A H. Effects of strontium and heat treatment on the wear-corrosion property of Al−7Si−0.3Mg alloy [J]. Materials Chemistry and Physics, 2012, 135(2/3): 503−509.
[22] FARAHANY S, OURDJINI A, BAKHSHESHI-RAD H R. Microstructure, mechanical properties and corrosion behavior of Al−Si−Cu−Zn−X (X=Bi, Sb, Sr) die cast alloy [J]. Transactions of Nonferrous Metals Society of China, 2016, 26 (1): 28−38.
[23] ÖZTÜRK I, HAPCI AĞAOĞLU G, ERZI E, DISPINAR D, ORHAN G. Effects of strontium addition on the microstructure and corrosion behavior of A356 aluminum alloy [J]. Journal of Alloys Compounds, 2018, 763: 384−391.
[24] DUYGUN İ K, HAPCI AĞAOĞLU G, DISPINAR D, ORHNA G. Time-dependent corrosion properties of Sr-modified AlSi9 alloy analyzed by electrochemical techniques [J]. Journal of Alloys and Compounds, 2019, 803: 786−794.
[25] OSORIO W R, GOULART P R, GARCIA A, SANTOS G A, NETO C M. Effect of dendritic arm spacing on mechanical properties and corrosion resistance of Al 9 wt pct Si and Zn 27 wt pct Al alloys [J]. Metallurgical and Materials Transactions A, 2006, 37(8): 2525−2538.
[26] ZOU Y C, YAN H, YU B B, HU Z. Effect of rare earth Yb on microstructure and corrosion resistance of ADC12 aluminum alloy [J]. Intermetallics, 2019, 110: 106487.
[27] Standard practice for preparing, cleaning and evaluating corrosion test samples [S]. American Society for Testing and Materials, ASTM G1-03, 2011.
[28] ASM Handbook. Alloy phase diagrams [M]. Materials Park, OH: ASM International, 1992: 248.
[29] ARTHANARI S, JANG J C, SHIN K S. Corrosion performance of high pressure die-cast Al−6Si−3Ni and Al−6Si−3Ni−2Cu alloys in aqueous NaCl solution [J]. Transactions of Nonferrous Metals Society of China, 2018, 28(11): 2181−2189.
[30] LASIA A, Electrochemical impedance spectroscopy and its applications [M]. New York: Springer, 2014.
[31] ARTHANARI S, JANG J C, SHIN K S. Corrosion performance of high pressure die-cast Al−Si−Mg−Zn alloys in 3.5 wt.% NaCl solution [J]. Journal of Alloys and Compounds, 2019, 783: 494−502.
[32] LIANG W J, ROMETSCH P A, CAO L F, BIRBILIS N. General aspects related to the corrosion of 6xxx series aluminium alloys: Exploring the influence of Mg/Si ratio and Cu [J]. Corrosion Science, 2013, 76: 119−128.
[33] TAHAMTAN S, BOOSTANI A F. Quantitative analysis of pitting corrosion behavior of thixoformed A356 alloy in chloride medium using electrochemical techniques [J]. Materials and Design, 2009, 30(7): 2483−2489.
[34] STAROSTIN M, SHTER G E, GRADER G S. Corrosion of aluminum alloys Al 6061 and Al 2024 in ammonium nitrate-urea solution [J]. Materials and Corrosion, 2016, 67(4): 387−395.
[35] ARTHANARI S, JANG J C, SHIN K S. Corrosion studies of high pressure die-cast Al−Si−Ni and Al−Si−Ni−Cu alloys [J]. Journal of Alloys and Compounds, 2018, 749: 146−154.
[36] CAVANAUGH M K, BIRBILIS N, BUCHHEIT R G, BOVARD F. Investigating localized corrosion susceptibility arising from Sc containing intermetallic Al_3Sc in high strength Al-alloys [J]. Scripta Materialia, 2007, 56(11): 995−998.

Al−6.5Si−0.45Mg−*x*Sc 铸造合金的显微组织及腐蚀行为

马玉坤，王明星，刘亚楠，蔡 彬

郑州大学 物理与微电子学院，材料物理教育部重点实验室，郑州 450001

摘 要：利用扫描电子显微术、X 射线衍射、电化学测量技术以及浸泡腐蚀实验，研究添加钪的 Al−6.5Si−0.45Mg 铸造合金的显微组织和腐蚀行为，并且与锶变质合金的实验结果进行比较。结果表明：钪对合金的初生 *α*(Al)相和共晶硅相有明显的细化和变质效果，随着钪含量的增加，效果增强。当钪含量增加到 0.58%(质量分数)时，钪对共晶硅相的变质效果几乎与锶的变质效果相当。与锶相比，钪可以改善实验合金在 NaCl 水溶液中的耐腐蚀性能，但过高的钪含量并不能进一步增强合金的耐蚀性。合金的腐蚀主要发生在合金的共晶区，且主要是共晶 *α*(Al)被溶解，这证实了共晶硅相比 *α*(Al)相具有更高惰性，并可在共晶硅与 *α*(Al)相之间形成腐蚀电池。

关键词：Al−Si−Mg 铸造合金；钪(Sc)；*α*(Al)相；共晶 Si 相；耐蚀性

(Edited by Xiang-qun LI)